PCCP

PAPER

View Article Online
View Journal | View Issue

Cite this: *Phys. Chem. Chem. Phys.*, 2023, **25**, 6203

Interaction mode of hydroxypropyl-β-cyclodextrin with vaccine adjuvant components Tween 80 and Triton X-100 revealed by fluorescence increasing-quenching analysis†

Yuya Kurosawa, Satoru Goto, * Kengo Mitsuya, Yuta Otsuka and Hideshi Yokoyama

The nonionic surfactants Tween 80 (Tw80) and Triton X-100 (TX100), which are used as components of adjuvants, were used with bovine serum albumin (BSA) and hydroxfypropyl-β-cyclodextrin (HP-β-CD) as model antigens. The interaction patterns of Tw80 and TX100 with the hydrophobic cores of the model antigens were investigated. The fluorescence of 8-anilinonaphthalene-1-sulfonic acid (ANS), a hydrophobic fluorescent probe, was used to evaluate the effect of surfactants on each model antigen. A Hanes Woolf plot was used to analyze the adsorption of ANS to BSA, and an activator–inhibitor model was used to analyze the concentration-dependent increase and decrease of ANS fluorescence intensity. For BSA, TX100 occupies the ANS binding site inside the BSA hydrophobic core, while Tw80 does not contribute to the ANS binding site in the hydrophobic core. For HP-β-CD, the ANS concentration required for analyzable fluorescence intensity extended to the range where ANS concentration-dependent quenching was not negligible. Using the activator inhibitor model, we were able to separate the activators and inhibitors of ANS fluorescence and evaluate the affinity of ANS for HP-β-CD and surfactants. The results obtained showed that TX100 provided a hydrophobic environment to the ANS while being encapsulated by HP-β-CD, while Tw80 did not interact with HP-β-CD and provided a hydrophobic environment to the ANS independently of each other. The interpretations obtained were corroborated by the determination of the CMC of TX100 and Tw80, the effect of salt on ANS fluorescence, and ^{1}H-NMR and ROESY. In summary, the results showed that the large hydrophilic head of Tween, composed of sorbitan and PEG chains, floated in the aqueous phase like a balloon, while Triton pierced the hydrophobic core of the antigen like a spear. In both BSA and HP-β-CD model antigens, TX100 impinged on the hydrophobic core.

Received 7th January 2023,
Accepted 17th January 2023

DOI: 10.1039/d3cp00094j

rsc.li/pccp

Introduction

Adjuvants are added to vaccines as components to enhance immune responses against antigens. However, the detailed mechanism of this has not been clarified. Therefore, we first focused on emulsion adjuvants, which have been used since ancient times. Emulsion adjuvants contain surfactants, components that may alter the conformation of antigenic proteins. In vaccines and other biopharmaceuticals, nonionic surfactants are used because they are generally considered not to alter the conformation of proteins.[1] But in fact, denaturation of proteins by nonionic surfactants has also been reported in many cases.[2] It has also been reported that Freund's adjuvant denatures rabbit sperm antigen and that rabbits immunized with Freund's adjuvant produced antibodies against the denatured antigen, antibodies against the native antigen, and multivalent antibodies.[3] The denaturation of antigens by adjuvant components should be considered important not only for the safety of vaccines but also for their efficacy. Related to this motivation, we have previously reported that sodium deoxycholate, used in oral vaccines, locally denatures the conformation of model antigens.[4]

In this study, we focused on Tween, Triton, and Span, which are nonionic surfactants widely used as adjuvant components. Of these, we used Tween 80 (Tw80), Tween 20 (Tw20), and Triton X-100 (TX100), whose hydrophilic–lipophilic balance (HLB) and cloud points are within the range of observable interactions with the model antigen. Tw80 and Tw20 have three hydrophilic PEG chains as the hydrophilic head from sorbitan. They are associated with a balloon-like shape due to the enormous

Faculty of Pharmaceutical Sciences, Division of Colloid and Surface Science, Research Institute for Science and Technology, Tokyo University of Science, 2641 Yamasaki, Noda, Chiba, 278-8510, Japan. E-mail: s.510@rs.tus.ac.jp

† Electronic supplementary information (ESI) available. See DOI: https://doi.org/10.1039/d3cp00094j

hydration volume of multiple PEG chains. TX100 is a surfactant with a basic skeleton of octylphenol ethoxylate and a spear-like structure with one hydrophilic head and one hydrophobic tail.

Interactions between surfactants and model antigens were examined using fluorescence spectroscopy, which is said to be 1000 times more sensitive than UV-vis spectroscopy,[5] and NMR spectroscopy, which has a sensitivity comparable to that of UV-vis spectroscopy. Bovine serum albumin (BSA), whose conformation and antigenicity in solution have long been studied in detail, was selected as the model antigen.[6,7] We also focused on cyclodextrin (CD) as a universal model for the hydrophobic core of the antigen, since CD has long been studied as a model for the substrate binding site of enzymes, starting with the publication of the book Einschlussverbindunger (Inclusion compounds) in 1954.[8] There are examples of utilizing CD derivatives as models for oxidases and esterases.[9,10] Recently, CD derivatives have been reported as models for lipases that can selectively hydrolyze lysophospholipids in hydrophobic cavities.[11] Thus, CD has been historically recognized as a model for the substrate binding site of enzymes, which is a typical example of an interface to external hydrophobic substances, and exploring how an adjuvant surfactant acts on it is believed to be an ideal experimental system that universally models the hydrophobic core of proteins. Using specific proteins such as BSA, ovalbumin (OVA), and ribonuclease (RNase) as antigen models does not allow us to escape from their unique properties,[12] and utilizing CD as a model of the hydrophobic core of the antigen may provide a solution to this problem. In this study, hydroxypropyl-β-cyclodextrin (HP-β-CD), which has a well-defined hydrophilic and hydrophobic surface and maximizes the fluorescence of the hydrophobic fluorescent probe (see below), was selected among cyclodextrins. The interaction between various nonionic surfactants and the model antigens, BSA and HP-β-CD, was evaluated by evaluating the adsorption and binding of the hydrophobic fluorescent probe to the hydrophobic core of the model antigen.

The hydrophobic core environment of BSA and HP-β-CD was evaluated by the fluorescence of 8-anilinonaphthalene-1-sulfonic acid (ANS), a hydrophobic fluorescent probe whose fluorescence is enhanced in hydrophobic environments or adsorbed in the lipid bilayer of liposomes, in the hydrophobic core of proteins,[13–17] or in the micelles of surfactants.[18] Therefore, ANS is used to evaluate the hydrophobic environment provided by these macromolecules and small molecules. However, the fluorescence intensity of ANS and other fluorescent molecules begins to decrease after a certain concentration. This is called concentration quenching, which is widely known as quenching due to the internal filter effect.[19] Other possible quenching mechanisms include Förster resonance energy transfer (FRET) and the Dexter mechanism,[20,21] which are caused by the proximity of fluorescent molecules to each other. Regardless of the mechanism, the quenching caused by the increase in the number of fluorescent molecules is an obstacle to the evaluation of the hydrophobic environment provided by medium and macromolecules. To solve this problem, we utilized the activator–inhibitor model in this study. The patterns on the shells of snails and clams contain a pattern with a fixed interval, such as a pattern that strongly emerges or, conversely, fades. The activator–inhibitor model is a mathematical model that can reproduce the increase and quenching of ANS fluorescence.

In summary, in this study, the hydrophobic fluorescent probe ANS was adsorbed and bound to model antigens such as BSA and HP-β-CD. There have been many fluorescence analyses of interactions between ANS and CD,[22,23] ANS and surfactants,[24,25] and CD and surfactants.[26] However, whether the ANS is provided with a hydrophobic environment by CDs or surfactants, the fluorescence spectrum of the ANS is not significantly different between the two, and therefore, a mixture of the three has not been studied extensively. We would like to emphasize that the activator-inhibitor model used in this study was able to clarify the behavior of CD and surfactant in a mixture of the three by analyzing both enhancement and decay of fluorescence intensity. The interactions between these surfactants and the hydrophobic core of the model antigen were investigated. The binding mode of the surfactant to the hydrophobic core of the antigen depending on the basic structure of the surfactant revealed in this study is very important for the optimization of the surfactant as a component of the adjuvant for the conformation of the antigen.

Experimental

Materials

BSA, HP-β-CD and Tween 20 were purchased from FUJI FILM Wako Pure Chemical Industries (Osaka, Japan). TX100 was purchased from NACALAI TESQUE (Kyoto, Japan), and Tw80 was purchased from Sigma-Aldrich (St. Louis, USA). ANS was purchased from Tokyo Chemical Industries (Tokyo, Japan). All other reagents were of the highest commercially available grade. The surfactants TX100, Tw80, and Tw20 were all used at 0.8 × their respective critical micelle concentration (CMC). CMC is 240 μM for TX100, 12 μM for Tw80, and 60 μM for Tw20, respectively.[27]

Fluorescence measurements

All fluorescence measurements were conducted using a Shimadzu RF-5300PC spectrofluorophotometer (Shimadzu, Kyoto, Japan). The excitation and emission slit widths were 5 nm each. The fluorescence spectrum was measured at an excitation wavelength of 390 nm. In the measurements, all solvents were 0.01 mol L^{-1} phosphate buffer (pH 6.8) prepared from potassium dihydrogen phosphate and natrium hydrogen phosphate.

Fluorescence analysis for adsorption of ANS on BSA

The amount of ANS adsorbed on BSA was evaluated by measuring the ANS fluorescence produced upon binding to BSA. The method is basically the same as previously described and is briefly described below.[28] Fig. S3A (ESI†) shows the intensity of ANS fluorescence in the presence of various concentrations of ANS in BSA. The original fluorescence spectrum is shown in Fig. S2 (ESI†). This saturation curve was curve-fitted with the

following equation to obtain the slope $I'(0) = B$ at the origin by differentiation.

$$I(C) = \frac{n'K'C}{1 + K'C} \quad (1)$$

$$I'(C) = \frac{n'K'^{(1+n'K')} - n'K'^2C}{(1 + K'C)^2} \quad (2)$$

This value of B exhibits the following relationship.

$$I = B\Gamma \quad (3)$$

where Γ is the amount of ANS bound to BSA (nM) and Γ per 1 M of BSA is the amount of ANS adsorbed γ. This procedure yielded the adsorption isotherm curve shown in Fig. 1A. The adsorption isotherm of ANS on BSA has been studied as Langmuir type adsorption, and we followed the Langmuir type analysis. Fig. 1B shows the Hanes–Woolf plot according to eqn (4) and Fig. S3B (ESI†) shows the Scatchard plot according to eqn (5).

$$\frac{C}{\gamma} = \frac{1}{n}C + \frac{1}{nK} \quad (4)$$

$$\frac{\gamma}{C} = -K\gamma + nK \quad (5)$$

Activator–inhibitor model for ANS fluorescence increasing-quenching analysis

The activator–inhibitor model is shown below.

$$\mathrm{AUC}\ (C) = A\ (e^{-k_iC} - e^{-k_aC}) \quad (6)$$

The area under the curve (AUC) is the sum of the fluorescence intensities of the ANS fluorescence spectra from 400–600 nm. C is the ANS concentration from 0–5000 μM. The k_i is the same for all samples, while A and k_a were fitted as values specific to each sample. The outline is shown in Fig. 2B.

Determination of stability constants for HP-β-CD of ANS

Fluorescence measurements applied to the determination of stability constants are based on the proportionality of fluorescence intensity to fluorophore concentration, $F = k_c$, where k is the proportionality constant, which incorporates the quantum yield and the absorptivity. Deviations from this linear relationship are common at higher concentrations as a consequence of the self-quenching phenomenon. In this study, consider the formation of the 1 : 1 complex SL between substrate (guest, ANS) S and ligand (host, HP-β-CD) L, with stability constant $K_{11} = [SL]/[S][L]$. Since HP-β-CD are nonfluorescent, the fluorescence intensity F is given by eqn (7).

$$F = k_s[S] + k_{11}[SL] \quad (7)$$

In the absence of CD, the fluorescence intensity is:

$$F_0 = k_s^0 S_t \quad (8)$$

where $S_t = [S] + [SL]$. The proportionality constants k_s and k_s^0 may in general be different. A combination of the above (7) and (8) relationships give eqn (9), which provides the basis for most of the fluorometric methods of stability constant estimation.[29]

$$\frac{F}{F_0} = \frac{k_s/k_s^0 + (k_{11}/k_s^0)K_{11}[L]}{1 + K_{11}[L]} \quad (9)$$

^{1}H NMR and ROESY measurements

^{1}H NMR and Rotating frame nuclear Overhauser Effect SpectroscopY (ROESY) measurements were conducted using a JNM-ECZ400S FT-NMR (FUJI FILM Wako Pure Chemical Industries, Osaka, Japan). The powder or liquid sample to be measured was dissolved in D_2O to a total of 20 mg.

Results and discussion

TX100 penetrates the BSA hydrophobic core, while Tw80 gently envelops the BSA hydrophobic core

Considering the interaction between surfactants and antigens *in vivo*, surfactants must exist *in vivo* at dilute concentrations that do not form micelles. First, we verified the concentration that can provide maximum hydrophobic tails to ANS and antigens at concentrations less than the CMC, and the results are shown in Fig. S1 (ESI†). Fig. S1A (ESI†) shows the ANS fluorescence spectra in the presence of various concentrations of TX100, and Fig. S1B (ESI†) shows the fluorescence intensity plotted against TX100 concentration, which is known as the determination of CMC by a fluorescence method.[30] The CMC of TX100 calculated from the intersection of the two approximate straight lines in Fig. S1B (ESI†) was 247 μM, which is in close agreement with the literature value. The CMC of Tw80 calculated from the intersection of two approximate straight lines in Fig. S1D (ESI†) was 10.6 μM, which is roughly in agreement with the literature value. In this study, TX100 and Tw80 were used at 192 μM and 9.6 μM, respectively, and the results so far indicated that both surfactants interact most effectively with ANS and increase the fluorescence intensity at these concentrations, which do not reach CMC.

Since nonionic surfactants interact with hydrophobic regions of proteins, we first followed the effect of nonionic surfactants on the fluorescence of ANS caused by binding to the hydrophobic regions of BSA in the presence of various surfactants. Although ANS has been reported to induce FRET with BSA, its binding to BSA has been studied in depth, and it has high affinity with other host molecules used as model antigens. Furthermore, unlike pyrene and DPH, ANS was used because it has a single fluorescent band that is easy to analyze. Fluorescence spectra of BSA alone and in the presence of Tw80 or TX100 and increasing ANS concentration are shown in Fig. S2A–C (ESI†). Only in the presence of BSA, the fluorescence at 470 nm was intensified with increasing ANS concentration. In addition, Fig. S2D and E (ESI†) show that surfactant alone hardly increases the fluorescence intensity of the ANS in the 0–800 nM range. A graph showing the amount of ANS adsorption to BSA on the vertical axis and the ANS concentration on the horizontal axis is shown in Fig. 1A. Since saturation curve-like results were obtained for all samples, a Hanes Woolf plot was created as

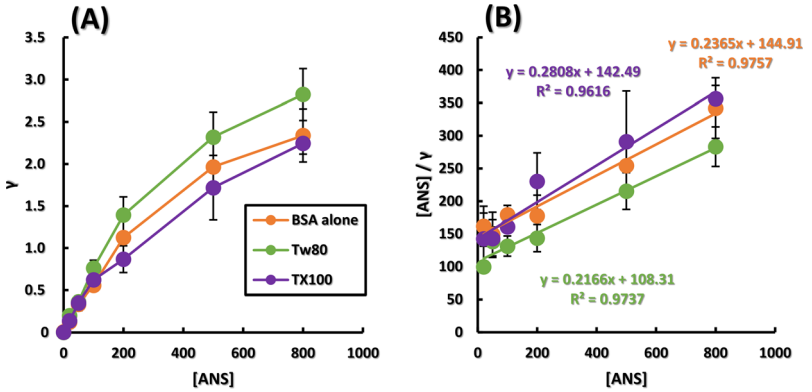

Fig. 1 TX100 obviously reduced the number of ANS bonds to BSA. (A) ANS adsorption amount with respect to the ANS initial concentration. (B) Hanes Woolf plot from (A) showing that the plot in (A) exists on the saturation curve. [BSA] = 100 nM, [Tw80] = 9.6 μM, [TX100] = 192 μM. The concentration of these surfactants is 0.8 times that of the respective CMC.

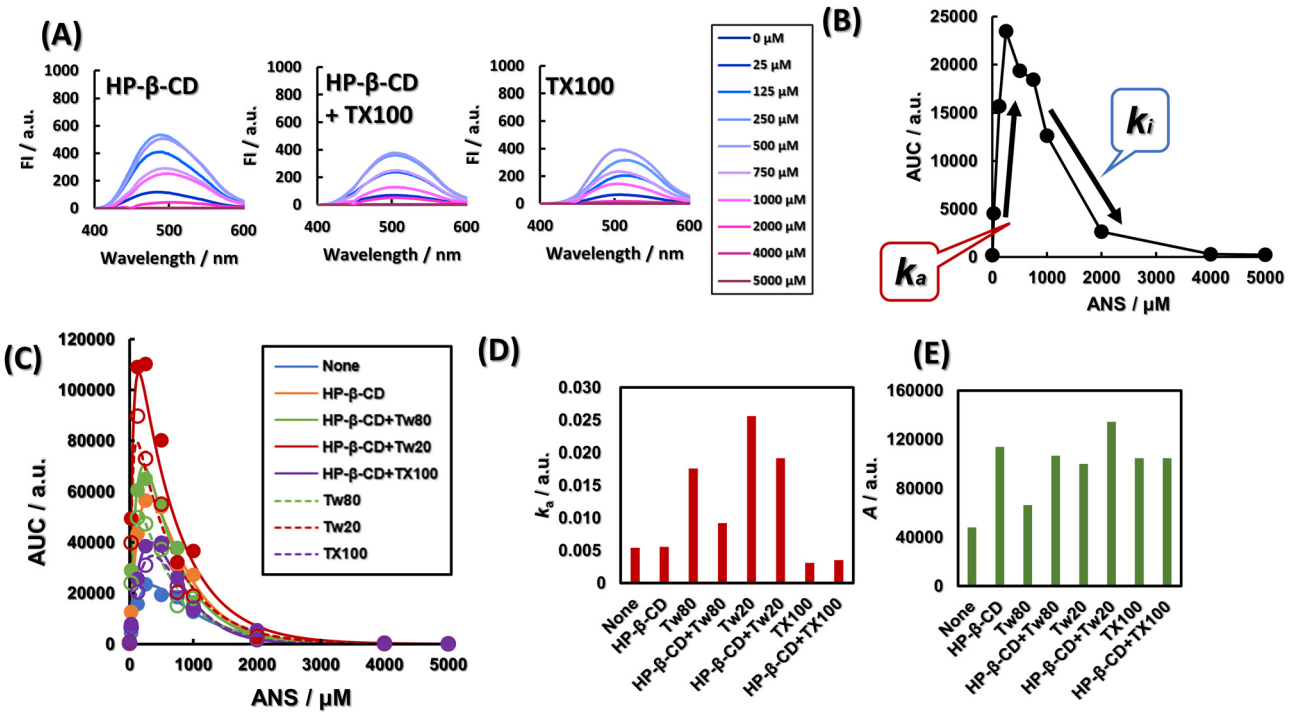

Fig. 2 Separation of fluorescence intensity increasing factor from fluorescence intensity decreasing factor by an activator inhibitor model. (A) ANS concentration-dependent generation of quenched ANS molecules in the presence of HP-β-CD, TX100, or both. (B) Outline of activator inhibitor model. k_a shows an increase in ANS incorporated into the hydrophobic region of HP-β-CD and surfactants, and an increase in the concentration of unquenched free ANS. k_i indicates aggregate formation of ANS. (C) ANS concentration-dependent generation of quenched ANS molecules in the presence of HP-β-CD, various non-ionic surfactants, or both. The plots are experimental values, and the decay curves are curve-fitted by the activator–inhibitor model. (D and E) The effects of nonionic surfactants on ANS fluorescence and HP-β-CD differ depending on their basic framework and hydrophobicity. k_a, k_i and A are values calculated from the activator inhibitor model. (D) k_a shows an increase in ANS incorporated into the hydrophobic region of HP-β-CD and surfactants, and an increase in the concentration of unquenched free ANS. k_i indicates aggregate formation of ANS. (E) A indicates the magnitude of AUC calculated from ANS fluorescence spectrum in the presence of HP-β-CD, various non-ionic surfactants, or both. [HP-β-CD] = 20 μM, [TX100] = 192 μM, [Tw80] = 9.6 μM. [Tw20] = 48 μM. The concentration of these surfactants is 0.8 times that of the respective CMC.

shown in Fig. 1B. The adsorption of Langmuir-type ANS to BSA was analyzed using a Hanes Woolf plot. Fig. S3B (ESI†) shows a Scatchard plot. The assumption of the Scatchard plot that the multiple sites are independent of each other cannot be guaranteed for BSA, a soft host whose conformation changes upon binding of small molecules. In addition, the Scatchard plot, which emphasizes the variability of the experimental values,[31] is effective when there is a host–guest relationship where chemisorption and physisorption are compatible, but as can be seen from the plots, this is not the case in the present study. The reliability of the parameters obtained from the Scatchard plot for Fig. S3B (ESI†), where the coefficient of determination is lower, is

Table 1 Number of binding sites n for BSA of ANS and association constant K obtained from the Hanes–Woolf plot in Fig. 1B

	n	$K/10^6$ M^{-1}
BSA alone	4.23	1.63
Tw80	4.62	2.00
TX100	3.56	1.97

low. Therefore, the Hanes Woolf plot with a higher coefficient of determination was used in this study. Table 1 shows the calculated number of ANS binding sites on BSA and the binding constants of ANS to BSA. Tw80 and TX100 increased the binding constant K by a factor of around 1.2. The number of binding sites n was significantly decreased for TX100, while it was almost unchanged for Tw80.

The increase in the binding constant K of ANS to BSA may be due to the increase in hydrophobicity of the hydrophobic core of BSA by Tw80 and TX100, creating a state in which ANS is more easily adsorbed. The decrease in the number of binding sites of ANS was caused by the addition of TX100, indicating that TX100 occupied some of the binding sites of ANS. Tw80 did not interfere with ANS access to the binding sites, suggesting that it increased the hydrophobicity of the BSA hydrophobic core by covering BSA. The results so far indicate that TX100 interacts with the hydrophobic core of BSA in a piercing manner in contrast to the bulky Tw80, indicating that the effect of nonionic surfactants on the hydrophobic core of antigen proteins is dependent on their basic backbone.

In a study on the binding of ANS to BSA, it was shown that there are about five binding sites for ANS in BSA.[32] The present results show that TX100 clearly occupies one of the ANS binding sites to BSA. Since the driving force of the interaction between the nonionic surfactant and the protein is a hydrophobic interaction, it can be inferred that this is the binding site of the ANS in the hydrophobic core of BSA. A study on the fluorescence of Trp residues intrinsic to BSA reported that Trp residues in the BSA hydrophobic pocket are buried by TX100 and Tw80.[33–35] It was also shown that TX100 acts only on Trp213 in the hydrophobic core of BSA,[36] while Tw80 acts only on Trp134 on the outside of BSA.[34] The burial of Trp residues was consistent with our interpretation of the increase in ANS association constant K, and the binding selectivity of TX100 and Tw80 for BSA was consistent with our interpretation that only TX100 reduced the number of ANS binding sites n. For more information, the study of the Förster distance between BSA intrinsic Trp residues and ANS revealed that the majority of ANS binding sites are localized around Trp213 of BSA.[16] It is also reported that the structure of Tw80 is so bulky that it can only partially form hydrogen bonds with the amino acid residues of BSA.[34] The less bulky and linear conformation of TX100 is assumed to be impinging on the hydrophobic core of BSA like a spear.

It is difficult to follow the hydrophobic core of the model antigen in detail in the experiments using the protein as the model antigen. Therefore, HP-β-CD was used as a model antigen.

Activator Inhibitor model showed TX100 is banded with HP-β-CD, while Tw80 is independent of HP-β-CD

Fig. 2A shows the fluorescence spectra of ANS at various concentrations in the presence of HP-β-CD, in the presence of HP-β-CD and TX100, and in the presence of TX100. As shown in Fig. S4 (ESI†), regardless of the presence of HP-β-CD and various surfactants, ANS showed a concentration-dependent fluorescence enhancement up to 250 μM and quenching at higher concentrations. To separate the factors that attenuate and enhance the fluorescence intensity, we applied the activator-inhibitor model, eqn (6), as outlined in Fig. 2B. The activator–inhibitor model, which has been used in studies of feather morphogenesis,[37] models the interaction of an activator and an inhibitor for a given event. It had been historically expressed as a linear differential equation whose solution is the sum of the exponential functions.[38] This is shown in eqn (6). The area under the curve (AUC) of various fluorescence spectra at 400–600 nm is expressed as a function of ANS concentration, as shown in Fig. 2A and Fig. S4 (ESI†). The addition of Tw80, Tw20, and TX100 increased the AUC. The AUCs of Tw80 and Tw20 were further increased by the addition of HP-β-CD, while the AUC of TX100 was almost unchanged. The parameters k_a and A obtained by fitting are shown in Fig. 2D and E, respectively. k_a is a constant reflecting the gradient of ANS fluorescence increase with ANS concentration, and A is the simple AUC increase, *i.e.*, the fluorescence quantum yield of ANS molecules, equalized by the ANS concentration. The addition of Tw80 and Tw20 increased k_a. The addition of TX100 decreased k_a, and the coexistence of HP-β-CD did not change k_a. Compared with ANS alone, A, which corresponds to the fluorescence quantum yield, increased when HP-β-CD, Tw80, Tw20, and TX100 were added in coexistence. The A of Tw80 and Tw20 increased with the coexistence of HP-β-CD, while that of TX100 increased with the coexistence of HP-β-CD. On the other hand, the A value of TX100 was almost constant regardless of the presence or absence of HP-β-CD.

The little difference between the k_a values of ANS alone and HP-β-CD may be due to the excess concentration of ANS, and does not indicate that HP-β-CD does not encapsulate ANS. In fact, the Jobs plot shown in Fig. S6 (ESI†) indicates the formation of a 1 : 1 complex between HP-β-CD and ANS, suggesting that HP-β-CD provides a hydrophobic environment for ANS, and that the difference in A between ANS alone and in the presence of HP-β-CD was more than 2-fold. Or Tw80 and Tw20 may be encapsulated by HP-β-CD, and ANS may lose the opportunity to be provided with a hydrophobic environment. The A of Tw80 and Tw20 is about one-half of that of HP-β-CD. A indicates the difference in polarity of the hydrophobic environment provided to ANS. This result indicates that HP-β-CD deprives the ANS of Tw80 or Tw20 and that HP-β-CD and Tw80 or Tw20 independently provide a hydrophobic environment for the ANS without interacting with each other. On the other hand, the k_a of TX100 was hardly changed by the addition of HP-β-CD. This result suggests that TX100 provides a hydrophobic environment to the ANS by its alkyl chains in the presence of HP-β-CD as well as in the absence of HP-β-CD.

Alternatively, TX100 and HP-β-CD may provide a hydrophobic environment for the ANS separately, without TX100 delivering the ANS to HP-β-CD. Here, the A value of TX100 was independent of the presence of HP-β-CD, suggesting that it is TX100 that provides the hydrophobic environment to the ANS even in the presence of HP-β-CD. This result strongly supports the former phenomenon. The application of the activator–inhibitor model to the fluorescence spectra provided a lot of information not only about the simple hydrophobicity around the ANS but also about the interaction mode between the nonionic surfactant and HP-β-CD.

From Fig. 2D and E, the height of k_a TX100 < Tw80 < Tw20, and the height of A is shown as Tw80 < Tw20 < TX100. The HLB of Tw20 and Tw80 is 15.0 and 16.7, respectively, and the HLB of TX100 is 13.5.[39] Here, the magnitude of k_a corresponds to the magnitude of HLB, *i.e.*, the hydrophilicity of the surfactant. The larger the percentage of PEG chains in the surfactant molecule, the greater the k_a affinity with ANS due to hydrogen bonding with secondary amines of ANS. Comparing Fig. S1B and D (ESI†) shows that the slope of the approximate curve before micelle aggregation is about 70 times higher for Tw80 than for TX100. The slope of this line is considered to indicate the magnitude of affinity between the monomer surfactant and the fluorescent probe,[30] and it can be seen that Tw80 has a higher slope, or affinity for ANS, than TX100. As shown above, k_a is more than five times larger for Tw80 than for TX100. This agreement also supports that k_a is a parameter that indicates affinity of ANS. The spear-like shape of TX100 is thought to provide a more densely hydrophobic environment for the ANS than the bulkier Tw80 and Tw20, leading to a larger A. The hydrophobic tail of Tw80 is longer than that of Tw20 by 6 ethyl groups and contains one double bond. The hydrophobic tail of Tw80 is six ethyl groups longer than that of Tw20 and contains one double bond. These two features indicate that Tw80 provides a sparser hydrophobic environment for the ANS than Tw20. Therefore, A, which would correspond to the quantum yield of ANS, would be determined by the sparsity of the hydrophobic environment provided to ANS. In this case, we assume a concentration where the surfactant is present as a monomer or incomplete aggregate and does not form micelles, but basically based on the idea of a critical filling parameter, which is a geometric model of the filling factor of the hydrophobic region of a micelle.[40]

In addition, the activator inhibitor model was applied to quantitatively observe the increase in ANS fluorescence intensity, which is derived from the peak intensity of the ANS fluorescence spectrum, which is subject to concentration quenching. The quenching can also be caused by internal filtering effects, FRET and Dexter mechanism, and the application of the activator inhibitor model can remove this quenching as k_i. There is a report that a method to correct the self-quenching of fluorescent molecules has been achieved by acquiring absorbance and fluorometer internal structure data.[41] The activator inhibitor model in this study is distinct in that it can accomplish this by simply measuring the fluorescence spectrum and there are no other parameters required. Also, the activator inhibitor model simplified the interpretation of complex fluorescence spectra that is difficult to interpret.

As can be seen in Fig. 2A and Fig. S4 (ESI†), the ANS fluorescence spectra show complex peak shifts with the concentration. Aggregation or interaction with CD or surfactants were considered as the cause of the shift of ANS fluorescence. We thought that aggregation of ANS with a long diameter of more than 1 nm[42] in monomers would be confirmed by DLS. However, since the presence of aggregates could not be confirmed by Dynamic Light Scattering (DLS) measurements, it was assumed that ANS behaved in the latter way. In Fig. S4 (ESI†), when only ANS was present, no ANS concentration-dependent wavelength shift was observed, and the peak wavelength was always 520 nm, indicating that the environment in which ANS was present did not depend on its concentration. In Fig. 2A, the peak wavelength of HP-β-CD was 485 nm at 25 μM ANS, and then shifted to 510 nm as the fluorescence intensity decreased. This indicates that the amount of free ANS is predominant over that provided by the hydrophobic environment. The peak wavelength was always maintained around 508 nm with HP-β-CD + TX100. The decrease in fluorescence intensity and the red shift caused by the addition of TX100 to HP-β-CD indicate that ANS was driven out of the HP-β-CD lumen and transferred to a more hydrophilic environment. In other words, HP-β-CD was considered to encapsulate TX100. In a study of β-CD mixed with anionic surfactant octylsulfate and ANS, quenching was observed when octylsulfate was added to a fixed concentration of β-CD and ANS. It is claimed that ANS and octylsulfate compete with each other for β-CD.[43] We hypothesized that the same thing is happening with HP-β-CD + TX100. In the presence of TX100 alone, the peak wavelength shifted to 508 nm at 25 μM ANS and to 517 nm at concentrations up to 250 μM. At higher concentrations, the peak wavelength shifted to 508 nm. This characteristic shift in peak wavelength was considered to be related to the affinity of TX100 for ANS. Here, when the ANS concentration was 25 μM, the addition of HP-β-CD to TX100 did not significantly change the fluorescence intensity and wavelength. This suggests that TX100 provides a hydrophobic environment for ANS in both systems, and that in the case of HP-β-CD + TX100, TX100 provides a hydrophobic environment for ANS in the HP-β-CD-incorporated state. Note that the addition of Tw80 to the HP-β-CD showed a slight redshift from 485 nm to 488 nm at a concentration of 25 μM ANS, while the addition of Tw80 to HP-β-CD increased the intensity of ANS fluorescence compared to HP-β-CD alone. The addition of Tw80 also increased the fluorescence intensity of ANS more than HP-β-CD alone. The wavelength shift indicated an increase in the polarity of the environment in which some ANS were present. In addition to this, the increase in fluorescence intensity suggests that the amount of ANS provided with a hydrophobic environment is increasing, *i.e.*, both Tw80 and HP-β-CD may be independently providing a hydrophobic environment for ANS. In the presence of Tw80 alone, the peak wavelength was 491 nm and the fluorescence intensity was more than twice that of HP-β-CD alone at an ANS concentration of 25 μM, and a slight increase in fluorescence intensity from

491 nm to 488 nm was observed in Tw80. The wavelength shift indicates that some ANS have migrated to a less polar environment, and the increase in fluorescence intensity indicates an increase in the amount of ANS being provided with a hydrophobic environment. Overall, it appears that both Tw80 and HP-β-CD independently provide a hydrophobic environment for ANS. The same trend was observed for Tw20.

The discussion on the fluorescence spectrum itself shows that even considering a single ANS concentration of 25 μM, the amount of information is so huge that the usefulness of the activator–inhibitor model, which provides concise information after adapting to all concentrations, can be better understood. To further solidify the interpretation of these results, we will now delve deeper into the factors that increase the fluorescence intensity of the ANS associated with k_a.

NaCl concentration-dependent increase in the uptake of ANS molecules by HP-β-CD and various nonionic surfactants

To clarify the phenomenon reflected by k_a, which shows a gradient of increase in ANS fluorescence with ANS concentration, we determined the ratio of ANS to HP-β-CD to determine how many times more intense ANS fluorescence was produced against HP-β-CD concentration than in the absence of HP-β-CD, as shown in Fig. 3A. The raw data of Fig. 3A shown in Fig. S5 (ESI†) confirm the concentration-dependent blueshift of the peak wavelength of HP-β-CD, indicating that ANS is indeed migrating inside the hydrophobic core of HP-β-CD. In Fig. 3A, the plots showed linearity regardless of the NaCl concentration. The slope increased with increasing NaCl concentration. The stability constants of ANS for HP-β-CD were calculated from these results and are shown in Fig. 3B. The stability constant K_{11} showed a linear increase with NaCl concentration. Next, we plotted the ANS fluorescence intensity against NaCl concentration in the presence of HP-β-CD, various nonionic surfactants, or both in the presence of ANS, as shown in Fig. 3C. Here, as shown in Fig. S7 (ESI†) which is the raw data of Fig. 3C, the fluorescence intensity may exceed the measurement limit in the presence of 0.8 M NaCl, and Fig. 3C. shows only HP-β-CD, Tw80 in the plot for 0.8 M NaCl. The slope of the graph, dFI/d[NaCL], which indicates the sensitivity of each sample to NaCl concentration, is shown on the vertical axis in Fig. 3D. The sensitivity of Tw80 to NaCl was increased by the addition of HP-β-CD, whereas that of TX100 was halved by the addition of HP-β-CD.

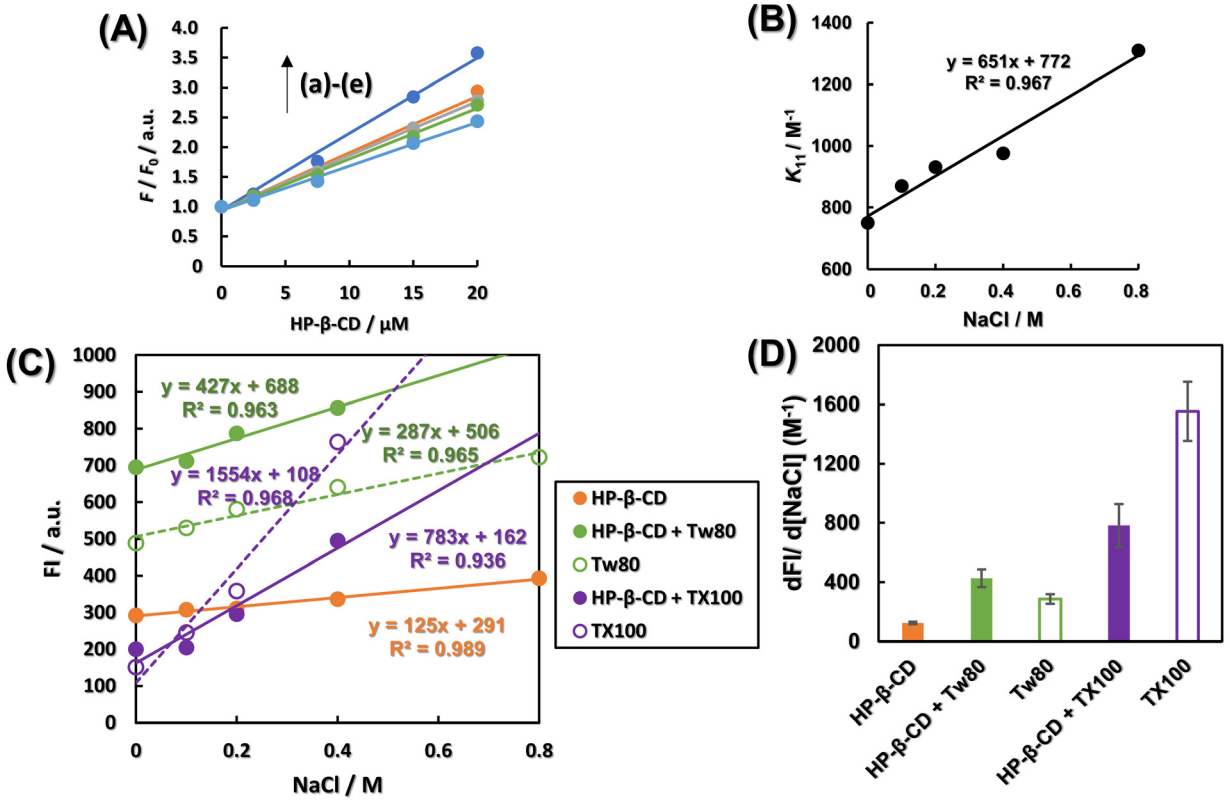

Fig. 3 Providing a hydrophobic environment to ANS in a NaCl concentration-dependent manner by HP-β-CD, Tw80 and TX100. (A) Linear increase of ANS fluorescence dependent on HP-β-CD concentration. The vertical axis is the fluorescence intensity at the peak top of the fluorescence spectrum. (a–e) 0, 0.1, 0.2, 0.4, 0.8 M NaCl, respectively. (B) NaCl concentration dependent linear increase in the stability constant of the HP-β-CD-ANS complex. [ANS] = 75 μM. Stability constants were calculated using eqn 9. For details, see experimental Section 4.3. (C and D) Response of ANS fluorescence to NaCl concentration in the presence of HP-β-CD, in the presence of surfactant, or in the presence of both. (C) The vertical axis is the fluorescence intensity of the fluorescence peak. [ANS] = 75 μM, [HP-β-CD] = 20 μM, [TX100] = 192 μM, [Tw80] = 9.6 μM. (D) The vertical axis is the slope of the change in fluorescence intensity in each sample against NaCl concentration: the slope of regression line in (A). Error bars indicate the standard deviation of the slope obtained from the multiple regression analysis. [ANS] = 75 μM.

In Fig. 3A, there was a linear relationship between the concentration of HP-β-CD and the increase in fluorescence intensity of ANS with HP-β-CD (F/F_0), indicating a 1 : 1 complex between ANS and cyclodextrin.[29] The 1 : 1 complex between ANS and HP-β-CD is also evident from the Job's plot shown in Fig. S6 (ESI†). The increase in the slope of the NaCl concentration-dependent line in Fig. 3A suggests an increase in the stability constant K_{11} in an NaCl concentration-dependent manner. The increase in NaCl concentration is a driving force for the aggregation of ANS, and the decrease in the solvent affinity of ANS due to the increase in the bulk polarizability is considered to have promoted the inclusion of ANS into HP-β-CD. In other words, it indicates that ANS salting out is inhibited by HP-β-CD. In Fig. 3C, the increase in the fluorescence intensity of ANS with increasing NaCl concentration in each sample is consistent with that of HP-β-CD. The increase in NaCl concentration may also promote aggregate formation of Tw80 and TX100,[44] which may provide a hydrophobic environment for the ANS and increase the fluorescence intensity of the ANS. For nonionic surfactants, the slope of Fig. 3C, *i.e.*, dFI/d[NaCl], reflects the degree of enhancement of aggregation by NaCl concentration; this value increased when HP-β-CD was added to Tw80 and decreased when HP-β-CD was added to TX100. The results for Tw80 indicate that the inclusion of ANS by HP-β-CD and the aggregation of Tw80 occur independently. The dFI/d[NaCl] values of HP-β-CD and Tw80 were summed up to 412, and the value of dFI/d[NaCl] for HP-β-CD + Tw80 was 427, indicating that additivity was established between the two. On the other hand, in the results of TX100, it was considered that this ''collar'' became a steric hindrance by inclusion of TX100 by HP-β-CD, and that the aggregation of TX100 was inhibited. It has been reported that β-CD increases the CMC of TX100, and clearly the present results reflect inhibition of TX100 aggregation.[43] In Fig. 3D, dFI/d[NaCl] is 2.3 times larger for HP-β-CD and Tw80, and 12.4 times larger for HP-β-CD and TX100. It is considered that dFI/d[NaCl] reflects two phenomena: the phenomenon that ANS cannot withstand the polarizability of the bulk and moves to the hydrophobic region, escaping from salting out, and the phenomenon that the hydrophobic region increases by the promotion of aggregation of nonionic surfactant. The dFI/d[NaCl] values for HP-β-CD reflect only the former, which is reflected in the dFI/d [NaCl] being small for HP-β-CD.

Fluorescence analysis with increasing NaCl concentration was able to strengthen the interpretation obtained by the activator–inhibitor model. However, it is only a hypothesis that TX100 is actually included in HP-β-CD and that Tw80 is not included in HP-β-CD. Therefore, the interaction between nonionic surfactant and HP-β-CD was verified more directly through evaluation of chemical shift value by one dimensional proton NMR measurement and observation of NOE by ROESY measurement.

TX100 places alkyl chains inside the hydrophobic core of HP-β-CD and PEG chains close to the HP groups of HP-β-CD

In order to clarify the interaction between TX100 and HP-β-CD and between Tw80 and HP-β-CD from a different point of view, one-dimensional proton NMR was first measured by changing the molar ratio of the two compounds. Fig. S8 (ESI†) shows the chemical shifts of the protons in the benzene ring of TX100 at 6.81 ppm and 7.18 ppm observed in TX100 alone, depending on the increase in the molar ratio of HP-β-CD. Fig. 4A shows the chemical shifts of each proton with respect to the molar ratio of HP-β-CD. Fig. 4A and B show the chemical shifts of the protons in the alkyl chain of TX100, which are 0.68 ppm, 1.26 ppm, and 1.63 ppm, respectively. Fig. S9 (ESI†) showed that no significant peak shift of the proton of Tw80 was observed depending on the molar ratio of HP-β-CD. Next, ROESY was measured to observe the proton proximity using the nuclear Overhauser effect (NOE). The results of the mixed sample of HP-β-CD and TX100 are shown in Fig. 4D, and those of the mixed sample of HP-β-CD and Tw80 are shown in Fig. 4E. From Fig. 4D, the coupling of the broad peak of the PEG chain of TX100 appearing at 3.4 to 4.0 ppm and the peak derived from $-CH_3$ of HP group of HP-β-CD appearing at 1.1 ppm was observed. In addition, the broad peak of the PEG chain of TX100 was observed to be coupled with the peak derived from H1′ and H1 existing outside the hydrophobic core of HP-β-CD appearing at 4.9 ppm and 5.1 ppm, respectively. From Fig. 4E, the coupling of the peak derived from H1′ existing outside the hydrophobic core of HP-β-CD appearing at 4.9 ppm and the peak derived from H4 of HP-β-CD appearing at 3.4 to 3.5 ppm was observed. In addition, the proximity of the protons of Tw80 and HP-β-CD and the interaction between them could not be observed here.

One-dimensional proton NMR measurements show that the down-field shift of the chemical shift values of the protons of TX100 depending on the mole fraction of HP-β-CD indicates an increase in hydrophobicity around the benzene ring and alkyl chains of TX100.[45] The lack of change in the chemical shift values of Tw80 as a function of the mole fraction of HP-β-CD confirms the absence of inclusion of Tw80 in HP-β-CD. The ROESY results indicated that not only the hydrophobic group of TX100 but also the hydrophilic PEG chain of TX100 interacted with the HP group of HP-β-CD, and that the PEG chain of TX100 wrapped around the HP group of HP-β-CD. The ROESY spectrum also shows that the PEG chains of TX100 interact with the outer H1′ and H1 of the hydrophobic core of HP-β-CD, suggesting that TX100 forms a stable complex with HP-β-CD through the interaction with both the inner and outer of the hydrophobic core of HP-β-CD. Fig. 4A and B show that the polarity around the protons of the alkyl chain and benzene ring of TX100 is reduced by the cavities in HP-β-CD. However, in the ROESY spectra shown in Fig. 4D, no NOEs were observed between the protons inside the HP-β-CD and the protons of these hydrophobic groups in TX100. This phenomenon has also been reported in studies on the inclusion of polyvinylpyrrolidone in γ-CD,[46] and given that NOEs are generally only detected when the distance between the protons is less than 4.5 Å, the alkyl chains and benzene rings of TX100 are not able to fit into the HP-β-CD cavity. CD, it is considered that TX100 wears HP-β-CD like a collar. The ROESY spectrum of Tw80 was evaluated at the depth where the coupling between the outer H1′ and H4 was more clearly observed, but the coupling between the protons from Tw80 and HP-β-CD was not confirmed, suggesting that HP-β-CD does not form a complex with Tw80.

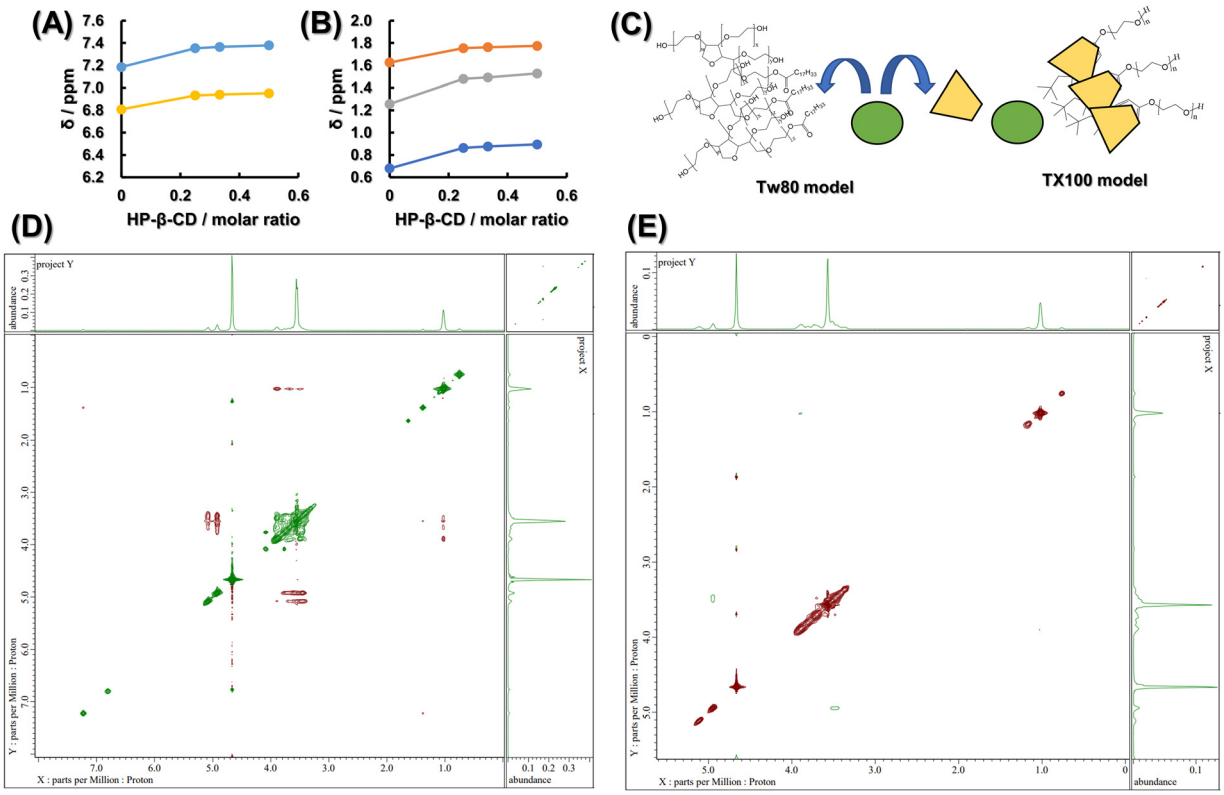

Fig. 4 TX100-specific interaction with HP-β-CD. HP-β-CD concentration-dependent shift of proton peaks in the benzene ring (A) and alkyl chain (B) of TX100. Scheme (C) shows that Tw80 provides a hydrophobic environment for ANS separately from HP-β-CD and TX100 with HP-β-CD as a necklace. ROESY spectra at various concentrations of HP-β-CD and TX100 (D) or Tw80 (E).

The results of both fluorescence and NMR analyses suggested the model shown in Fig. 4C, in which TX100 bound to BSA and HP-β-CD in a piercing manner, while Tw80 bound loosely and did not show active proximity. The bulkiness and the stickiness of TX100 and Tw80 can be easily imagined from the molecular model shown in Scheme S1 listed in the ESI.†

Conclusions

In the adsorption of ANS to BSA, TX100 and Tw80 both increased the affinity of ANS for BSA, while only TX100 took away the number of ANS binding sites. This was found to be due to TX100 impinging on ANS binding sites around the hydrophobic core where Trp213 of BSA resides. However, there is no guarantee that the relationship between multiple binding sites is independent for a soft host such as BSA, and the unique nature of BSA cannot be ignored. Therefore, we focused on the interaction of HP-β-CD with TX100 and Tw80 as a universal model of the hydrophobic pocket of the protein. In HP-β-CD, the concentration of ANS at which sufficient fluorescence was obtained was tens of times higher than that of BSA. The problem was the self-quenching of ANS at high concentrations. We utilized the activator–inhibitor model to separate the concentration-dependent ANS self-quenching from the enhancement of ANS fluorescence by HP-β-CD and surfactants as an activator and inhibitor. The fluorescence spectra themselves were very difficult to understand because the systems containing HP-β-CD and surfactants showed complex peak shifts with ANS concentrations. However, the parameter k_a calculated from the activator–inhibitor model, which was applied to all concentrations, made it easy to understand that TX100 penetrates HP-β-CD and Tw80 is independent of HP-β-CD. Each parameter and the interpretations obtained from them were corroborated by the determination of the CMC of TX100 and Tw80, the effect of salt on ANS fluorescence, ^{1}H-NMR and ROESY. As a result, HP-β-CD, which was chosen as the universal model, showed that only TX100 impinged on the hydrophobic core, as did BSA.

The use of HP-β-CD as a universal model of the hydrophobic pocket of antigenic proteins may contribute to accelerated optimization of the basic framework of surfactants used in adjuvants. The activator–inhibitor model can also simplify information in complex environments with multiple hosts, even when fluorescent molecules are required at concentrations high enough to cause self-quenching. This procedure would be expected to play an active role in the pharmaceutical field, where multiple macromolecules such as liposomes, micelles, and antibodies are intermingled, and to provide new insights.

Author contributions

Y. K. performed the experiments and analysed data and wrote the manuscript. S. G. is the supervisor of this work. Y. O., K. M. and H. Y. reviewed and edited the manuscript.

Conflicts of interest

There are no conflicts to declare.

Acknowledgements

The author would like to thank Dr. Tomohiro Tsuchida from Shiga University of Medical Science for his valuable comments and Dr. Motoo Iida from Tokyo University of Science for him skilled technical assistances.

Notes and references

1 T. A. Khan, H. C. Mahler and R. S. K. Kishore, Key interaction of surfactants in therapeutic protein formulations: A review, *Eur. J. Pharm. Biopharm.*, 2015, **97**, 60–67.
2 M. R. Peña, R. O. Nuñez, T. Pons, S. R. W. Louro and A. P. Gramatges, Physico-chemical studies of molecular interactions between non-ionic surfactants and bovine serum albumin, *Colloids Surf., B*, 2010, **75**, 282–289.
3 K. V. Barinova, E. V. Khomyakova, M. L. Kuravsky, E. V. Schmalhausen and V. I. Muronetz, Denaturing action of adjuvant affects specificity of polyclonal antibodies, *Biochem. Biophys. Res. Commun.*, 2017, **482**, 1265–1270.
4 Y. Kurosawa, Y. Otsuka and S. Goto, Increased selectivity of sodium deoxycholate to around Tryptophan213 in bovine serum albumin upon micellization as revealed by singular value decomposition for excitation emission matrix, *Colloids Surf., B*, 2022, **212**, 112344.
5 S. Zhu, T. Fischer, W. Wan, A. B. Descalzo and K. Rurack, Luminescence Amplification Strategies integrated with Microparticle and Nanoparticle Platforms, in *Luminescence Applied in Sensor Science*, ed. L. Prodi, M. Montalti, N. Zaccheroni, Springer, 2011, pp. 64–104.
6 M. Chruszcz, K. Mikolajczak, N. Mank, K. A. Majorek, P. J. Porebski and W. Minor, Serum albumins-Unusual allergens, *Biochim. Biophys. Acta*, 2013, **1830**, 5375–5381.
7 P. Restani, C. Ballabio, A. Cattaneo, P. Isoardi, L. Terracciano and A. Fiocchi, Characterization of bovine serum albumin epitopes and their role in allergic reactions, *Allergy*, 2004, **59**, 21–24.
8 R. Breslow and S. D. Dong, Biomimetic Reactions Catalyzed by Cyclodextrins and Their Derivatives, *Chem. Rev.*, 1998, **98**, 1997–2011.
9 T. H. Fenger and M. Bols, Simple cyclodextrin aldehydes as excellent artificial oxidases, *J. Inclusion Phenom. Macrocyclic Chem.*, 2011, **69**, 397–402.
10 A. Fragoso, R. Cao and M. Baños, Esterase activity of cyclodextrin dithiocarbamates, *Tetrahedron Lett.*, 2004, **45**, 4069–4071.
11 Y. Lee and N. K. Devaraj, Lipase mimetic cyclodextrins, *Chem. Sci.*, 2021, **12**, 1090.
12 A. Kondo, S. Oku and K. Higashitani, Structural changes in protein molecules adsorbed on ultrafine silica particles, *J. Colloid Interface Sci.*, 1991, **143**, 214–221.
13 J. R. Lakowicz, Solvent and Environmental Effect, in *Principles of Fluorescence Spectroscopy*, ed. J. R. Lakowicz, Springer, 2006, pp. 205–235.
14 M. R. Eftink, Fluorescence Methods for Studying Equilibrium Macromolecule-Ligand Interactions, in *Methods in Enzymology, Fluorescence Spectroscopy*, ed. L. Brand and M. L. Johnson, Academic Press, 1997, vol. **278**, pp. 221–257.
15 D. Matulis, C. G. Baumann, V. A. Bloomfield and R. E. Lovrien, 1-Anilino-8-naphthalene sulfonate as a protein conformational tightening agent, *Biopoly*, 1999, **49**, 451–458.
16 D. M. Togashi and A. G. Ryder, A Fluorescence Analysis of ANS Bound to Bovine Serum Albumin: Binding Properties Revisited by Using Energy Transfer, *J. Fluoresc.*, 2008, **18**, 519–526.
17 A. Hawe, M. Sutter and W. Jiskoot, Extrinsic Fluorescent Dyes as Tools for Protein Characterization, *Pharm. Res.*, 2008, **25**, 1487–1499.
18 M. Qiao, L. Ding and F. Lv, Surfanctant assebblies encapsulating fluorescent probes as selective and discriminative sensor for metal ions, *Coord. Chem. Rev.*, 2021, **432**, 213696.
19 J. R. Lakowicz, Quenching of Fluorescence, in *Principles of Fluorescence Spectroscopy*, ed. J. R. Lakowicz, Springer, 2006, pp. 278–330.
20 J. R. Lakowicz, Energy Transfer, in *Principles of Fluorescence Spectroscopy*, ed. J. R. Lakowicz, Springer, 2006, pp. 443–476.
21 J. R. Lakowicz, Mechanisms and Dynamics of Fluorescence quenching, in *Principles of Fluorescence Spectroscopy*, ed. J. R. Lakowicz, Springer, 2006, pp. 331–352.
22 B. D. Wagner and S. J. Fitzpatrick, A Comparison of the Host–Guest Inclusion Complexes of 1,8-ANS and 2,6-ANS in Parent and Modified Cyclodextrins, *J. Inclusion Phenom. Macrocyclic Chem.*, 2000, **38**, 467–478.
23 B. D. Wagner and P. J. MacDonald, The fluorescence enhancement of 1 -anilinonaphthalene-8-sulfonate (ANS) by modified P-cyclodextrins, *J. Photochem.*, 1998, **114**, 151–157.
24 C. J. Efaselle and D. B. Millar, Studies on Triton X-100 detergent micelles, *Biophys.*, 1975, **3**, 355–361.
25 E. D. Vendittis, G. Palumbo, G. Parlato and V. Bocchini, A Fluorimetric Method for the Estimation of the Critical Micelle Concentration of Surfactants, *Anal. Biochem.*, 1981, **115**, 278–286.
26 V. K. Smith, T. T. Ndou, M. D. L. Peña and I. M. Warner, Spectral characterization of β-Cyclodextrin: Triton X-100 complexes, *J. Inclusion Phenom. Macrocyclic Chem.*, 1991, **10**, 471–484.
27 D. Linke, Detergents: An Overview, in *Methods in Enzymology, Guide to Protein Purification*, ed. R. R. Burgess, M. P. Deutscher, Academic Press, 2009, ch. **34**, vol. 463, pp. 603–617.
28 M. Möller and A. Denicola, Study of Protein-Ligand Binding by Fluorescence, *Biochem. Mol. Biol. Educ.*, 2002, **30**, 309–312.
29 K. A. Connors, Measurement of Cyclodextrin Complex Stability Constants, in *Comprehensive Supermolecular Chemistry*, ed. J. L. Atwwod, Springer, 1996, pp. 205–242.

30 R. Wu, M. Tian, C. Shu, C. Zhou and W. Guan, Determination of the critical micelle concentration of surfactants using fluorescence strategies, *Soft Matter*, 2022 **18**, 8920.
31 D. D. Keightley, R. J. Fisher and N. A. C. Cressie, Properties and interpretation of the woolf and Scatchard plots in analysing data from steroid receptor assays, *J. Steroid Biochem.*, 1983, **19**, 1407–1412.
32 S. De, A. Girigowami and S. Das, Fluorescence probing of albumin-surfactant interaction, *J. Colloid Interface Sci.*, 2005, **285**, 562–573.
33 S. K. Singh and N. Kishore, Thermodynamic Insights into the Binding of Triton X-100 to Globular Proteins: A Calorimetric and Spectroscopic Investigation, *J. Phys. Chem. B*, 2006, **110**, 9728–9737.
34 M. Ruiz-Peña, R. O. Nuñez, T. Pons, S. R. W. Louro and A. P. Gramatges, Physico-chemical studies of molecular interactions between non-ionic surfactants and bovine serum albumin, *Colloids Surf., B*, 2010, **75**, 282–289.
35 N. M. Zadymova, G. P. Yampol'skaya and L. Y. Filatova, Interaction of Bovine Serum Albumin with Nonionic Surfactant Tween 80 in Aqueous Solutions: Complexation and Association, *Colloid J.*, 2006, **68**, 162–172.
36 I. M. Vlasova, A. A. Vlasov and A. M. Saletskii, Complexation of serum albumins and Triton X-100: Quenching of tryptophan fluorescence and analysis of the rotational diffusion of complexes, *Russ. J. Phys. Chem.*, 2016, **90**, 1479–1483.
37 M. P. Harris, S. Williamson, J. F. Fallon, H. Meinhardt and R. O. Prum, Molecular evidence for an activator-inhibitor mechanism in development of embryonic feather branching, *Proc. Natl. Acad. Sci. U. S. A.*, 2005, **102**, 11734–11739.
38 A. M. Turing, THE chemical basis of morphogenesis, *Bull. Math. Biol.*, 1990, **52**, 153–197.
39 J. M. Neugebauer, Detergents: An Overview, in *Methods in Enzymology*, ed. M. P. Deutscher, Elsevier, pp. 239–253.
40 J. N. Israelachvili, *Soft and Biological Structures, in Intermolecular and Surface Forces*, ed. J. N. Israelachvili, Elsevier, 2011, pp. 535–576.
41 A. Kasparek and B. Smyk, A new approach to the old problem: Inner filter effect type I and type II in fluorescence, *Spectrochim. Acta, Part A*, 2018, **198**, 297–303.
42 Z. Sun, L. Jin, W. Shi, M. Wei, D. G. Evans and X. Duan, Controllable Photoluminescence Properties of an Anion-Dye-Intercalated Layered Double Hydroxide by Adjusting the Confined Environment, *Langmuir*, 2011, **27**, 7113–7120.
43 J. W. Park and H. J. Song, Association of Anionic Surfactants with/3-Cyclodextrin. Fluorescence-Probed Studies on the 1:1 and 1:2 Complexation, *J. Phys. Chem.*, 1989, **93**, 6454–6458.
44 H. Maeda, S. Muroi and R. Kakehashi, Effects of Ionic strength on the Critical Micelle Concentration and the Surface Excess of Dodecyldimethylamine Oxide, *J. Phys. Chem. B*, 1997, **101**, 7378–7382.
45 Y. Saito, H. Ueda, M. Abe, T. Sato and S. D. Christian, Inclusion complexation of Triton X-100 with α-, β- and γ-cyclodextrins, *Colloids Surf., A*, 1998, **35**, 103–108.
46 T. Asada, K. Iguchi, T. Ueda, H. Kitagishi and K. Kano, Improvement of Hairstyling Performance by Inclusion Complexes with Cyclodextrins, *J. Soc. Cosmet. Chem. Jpn.*, 2014, **48**, 177–183.